Journal of Alloys and Compounds 495 (2010) 659–662

Contents lists available at ScienceDirect

Journal of Alloys and Compounds

journal homepage: www.elsevier.com/locate/jallcom

Formation and hydrogen reactivity of MgCo compound

M.G. Verón [a], F.C. Gennari [a,b,*]

[a] Instituto Balseiro (Universidad Nacional de Cuyo), Centro Atómico Bariloche, 8400 S.C. de Bariloche, Argentina
[b] Consejo Nacional de Investigaciones Científicas y Técnicas (CONICET), Instituto Balseiro (Universidad Nacional de Cuyo), Centro Atómico Bariloche, 8400 S.C. de Bariloche, Argentina

ARTICLE INFO

Article history:
Received 16 July 2008
Received in revised form 19 October 2009
Accepted 20 October 2009
Available online 29 October 2009

Keywords:
Complex hydrides
Hydrogen storage
Mechanical alloying
Kinetics

ABSTRACT

The Mg–Co mixture was milled using a low energy mill during 200 h under argon and then submitted to thermal treatment. The mechanical milling (MM) of Mg–Co mixture leads to microstructural refinement reducing the diffusion distances and then favoring the kinetics of solid-state reaction. As a consequence, the formation of MgCo compound occurs at temperatures of 573 K which is lower than previously reported. As-milled sample (Mg and Co phases) and as-milled plus heated sample (with mainly MgCo compound) were non-isothermally heated under hydrogen pressure using high-pressure differential scanning calorimetric equipment. The presence of MgCo intermetallic compound improves the reactivity with hydrogen, reducing both hydrogen absorption and desorption temperature, as well as increasing the total hydrogen storage capacity. An analysis of the interplay of hydride phases as a function of the starting samples and experimental conditions is presented.

1. Introduction

Mechanical milling/alloying is a powerful technique used for the refining/synthesis of different materials, in particular alloys and intermetallic compounds. Cold welding and fracturing mechanisms allow the formation of homogeneous alloys and intermetallics from metals with very different melting points, which are hard to produce by the traditional metallurgical processes. In the Mg–Co system, $MgCo_2$ is the only stable intermetallic compound reported [1,2]. However, a deep analysis of the literature and additional experimental evidence [3–7] corroborate the existence of MgCo intermetallic in the Mg-rich zone. Although the MgCo compound has not been formed during milling of the Mg–Co mixtures, further heating of as-milled mixtures leads to the formation of MgCo by solid-state diffusion [5–7]. In addition, MgCo intermetallic compound has been obtained after β-Mg_2CoH_5 and/or $Mg_6Co_2H_{11}$ decomposition [3–5,7]. Then, the understanding of the experimental conditions and kinetics constrains which favoring the MgCo formation is a key issue for the production of Mg–Co hydrides, such as Mg_2CoH_5 and $Mg_6Co_2H_{11}$, with promising properties for hydrogen storage applications. In this work the interplay between high-pressure differential scanning calorimetry and XRD diffraction allows to analyze the role of MgCo in the formation of complex hydrides at 573 K. The relation between the reactivity of the Mg–Co mixture with hydrogen, the influence of MgCo presence on the hydride phase formation and the changes of the hydride phases during cycling will be discussed.

2. Experimental

2.1. Synthesis

Starting materials were elemental powders of Mg and Co (purity of 99.9%). A mixture of 1:1 Mg–Co powders and ferromagnetic steel balls were placed in a stainless steel container that was closed within an argon dry box. The powders were milled up to a total time of 200 h using the Uni-Ball-Mill II apparatus (Australian Scientific Instruments). The final sample is hereafter indicated as MM200. The milling processes proceeded in a stationary argon atmosphere. The ball to powder weight ratio selected was 44:1. All handling of the powders was performed in a glove box under purified argon atmosphere.

MgCo intermetallic synthesis was performed using the Mg–Co mixture milled during 200 h (MM200). The as-milled sample was placed in an aluminum capsule and closed hermetically in a dry glove box. After this, the aluminum capsule was placed quartz in the tube and outgassed using mechanical vacuum for half an hour at room temperature. Then, the tube was sealed and heated up to 573 K during 5 days. After that, the aluminum capsule was recovered by breaking the quartz tube at room temperature under air atmosphere. Hereafter this sample is designed as MM200H.

2.2. Characterization

The crystalline structure of the samples was characterized by X-ray diffraction (XRD) on a Philips PW 1710/01 instrument with Cu Kα radiation (graphite monochromator). The crystalline size was calculated using Scherrer equation. The microstructure and Mg–Co distribution was studied by scanning electron microscopy (SEM 515, Philips Electronic Instruments) on resin-mounted and polished samples. The thermal behavior was investigated by high-pressure differential scanning calorimeter (HP-DSC, TA Instrument 2910 calorimeter) using a heating rate of 5 K min^{-1}. Absorption cycles were performed heating up to 573 K under 2 MPa of hydrogen pressure and kept at this temperature for 1 h. Desorption cycle was measured heating up to 673 K under vacuum and kept at this temperature for 0.5 h. The

* Corresponding author at: Centro Atómico Bariloche (CNEA), R8402AGP, S.C. de Bariloche, Argentina. Tel.: +54 2944 445118; fax: +54 2944 445190.
E-mail address: gennari@cab.cnea.gov.ar (F.C. Gennari).

0925-8388/$ – see front matter © 2009 Elsevier B.V. All rights reserved.
doi:10.1016/j.jallcom.2009.10.174

amount of hydride phase was estimated from the DSC curves, using the peak area and the mass of sample ($J\,g^{-1}$).

Pressure-composition isotherm (PCI) at 623 K was obtained using a modified Sieverts-type device, coupled with a mass flow controller [8]. The as-milled sample was heated up to the reaction temperature under vacuum and kept at this temperature for 30 min before hydrogen reaction. The reported PCI curve corresponds to the first absorption/desorption cycle.

3. Results and discussion

Mechanical milling of Mg–Co is a powerful technique for powder processing that improves diffusion distances and mixing. The repeated welding together of particles and fracture accompanying ball/powder collisions enable the creating of new surfaces during milling. Fig. 1 shows the agglomerate morphology of Mg–Co mixture after 200 h under argon (backscattered electrons), where Co particles are dispersed in the Mg matrix. The analysis of numerous agglomerates shows a reduction in the size distribution from 150 to 400 μm for starting Mg to a final agglomerate size of 5–150 μm. In addition, a good intermixing between Mg and Co is observed, with Co particles smaller than 10 μm (bright phase). The XRD pattern of MM200 (Fig. 2a) shows the peaks of magnesium (JCPDS Powder Diffraction Data Card No. 35-0821) and Co (JCPDS Powder Diffraction Data Card No. 5-0727). For both phases, the crystallite sizes were reduced to nanometric range, i.e. to a final size of 10 and 15 nm for Mg and Co, respectively. In addition, no new phases were formed due to the milling process, such as MgCo or $MgCo_2$ intermetallics. Then, the main effects of Mg–Co milling were improvement of Mg–Co intermixing, microstructure refinement and reduction in the agglomerate size distribution.

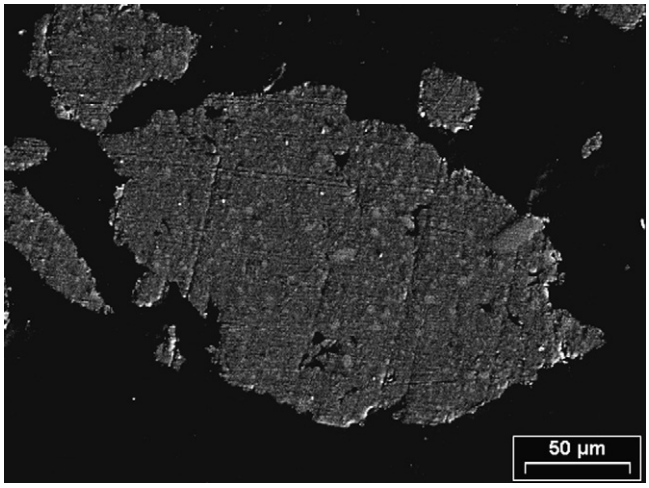

Fig. 1. SEM image of Mg–Co mixture after 200 h of milling under Ar (MM200).

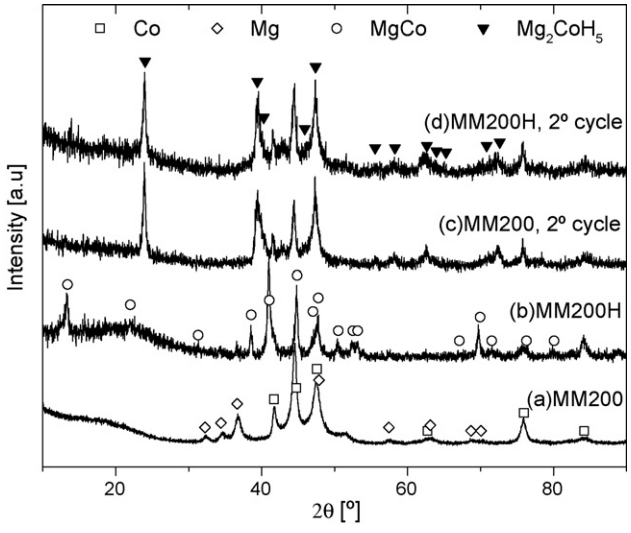

Fig. 2. X-ray diffraction patterns of (a) MM200; (b) MM200H; (c) MM200 after HP-DSC second absorption cycle; and (d) MM200H after HP-DSC second absorption cycle.

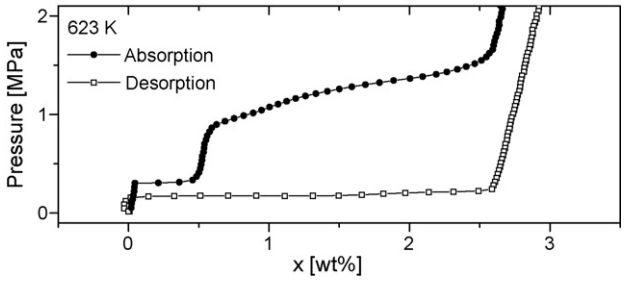

Fig. 3. Absorption/desorption PCI under static conditions at 623 K.

Heating of the MM200 sample for 5 days at 573 K (MM200H) introduces structural modifications in the sample. Fig. 2b shows mainly the characteristic diffraction pattern of MgCo intermetallic (JCPDS Powder Diffraction Data Card No. 44-1149) [5,6]. This novel result evidences that the formation of MgCo is possible by solid-state diffusion at temperatures as low as 573 K when Mg–Co contacting is improved (Fig. 1). No formation of $MgCo_2$ is detected, as is indicated by the absence of the peaks at $2\theta = 21.08^\circ$ and 48.93° (JCPDS Powder Diffraction Data Card No. 29-0486).

Absorption/desorption pressure-composition isotherm (PCI) at 623 K of the MM200 sample is shown in Fig. 3 (first cycle). The total hydrogen storage capacity of MM200 is about 2.6 wt.%, indicating the practically complete hydrogenation of the sample. Hydrogen absorption occurred in two stages given by well-defined plateaus: a flat one at 311 kPa and a sloped one developed between 915 and 1588 kPa. On the contrary, during desorption only one plateau can be identify at about 178 kPa. Then, the MM200 sample exhibits a strong hysteresis during hydrogen absorption/desorption process. This result is in agreement with our previous results [9–11], where from XRD analysis each plateau was associated with the formation of $Mg_6Co_2H_{11}$ and Mg_2CoH_5 hydrides. However, no thermodynamic information has been reported for Mg–Co mixture with 1:1 composition.

The kinetics behavior of Mg–Co–H system is complex. Different hydride phases have been formed due to the interplay between temperature, hydrogen pressure and time [3–7,9–12]: MgH_2, Mg_2CoH_5 and $Mg_6Co_2H_{11}$. In addition, factors such as Mg–Co mixture composition, the presence of MgCo intermetallic and microstructural/structural characteristic of the Mg–Co powder mixture have not been discarded. To determine the reactivity with hydrogen of the MM200 and MM200H samples and to provide information about the role of MgCo intermetallic on the kinetics formation of different hydrides in the Mg–Co–H, a study using HP-DSC measurements was performed. From the thermodynamic information obtained for MM200 during first cycle (Fig. 3), a hydrogen pressure of 2 MPa was selected as enough to allow the formation of any hydride phase at 573 K.

HP-DSC curves in Fig. 4 correspond to the first and second cycles of hydrogen absorption for the MM200 (Fig. 4A) and MM200H (Fig. 4B) samples, respectively. As can be seen from each sample, the cycling and the MgCo presence significantly influence the kinetics of the absorption reaction, which is indicated by a shift of absorption peaks towards higher/lower temperatures as a function of starting sample. The first cycle for MM200 is considered

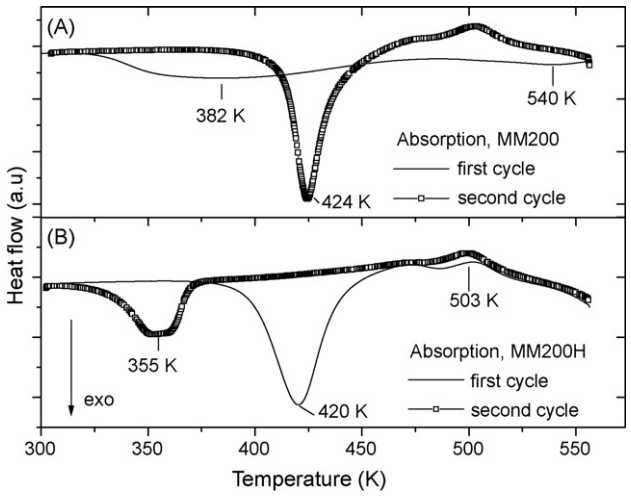

Fig. 4. HP-DSC curves during absorption reaction of MM200 (A) and MM200H (B). First cycle (—); second cycle (–□–). Heating rate 5 K min^{-1}; 2 MPa of H_2.

as an activation step, in similar way to reference [13]. For MM200 sample (Fig. 4A) two broad exothermic peaks are observed. The temperature of first peak shifts from 382 to 424 K, whereas the starting temperature of second peak does not change with cycling. Moreover, the heat flow involved in the first peak (1.6 J g^{-1}) is duplicated from the first to second cycle (2.9 J g^{-1}). On the other hand, the hydrogen reactivity of MM200H sample (Fig. 4B) is characterized by a sharp exothermic peak at 420 K which shifts to 355 K after cycling. In this case the heat flow involved in the first peak is reduced about 1/3 with cycling (from 2.9 to 1.1 J g^{-1}). In addition, in several cycles an endothermic peak at 503 K is clearly identified. It is associated with the structural transition of Mg_2CoH_5 from tetragonal to cubic. The slight temperature increase observed respect to the reported temperature of 488 K [3,4] is due to the hydrogen pressure effect. In the case of desorption step for MM200 and MM200H samples (Fig. 5), an important reduction in the hydride temperature decomposition is observed for MM200H sample (520 K) respect of MM200 (620 K).

The diffraction patterns of the final phases obtained after cycling for MM200 and MM200H are shown in Fig. 2 (curves c and d, respectively). The Mg_2CoH_5 phase is the only hydride phase detected after second absorption cycle independently of the starting sample. Simultaneously, residual Co phase is also observed in correlation with the Mg/Co composition. No MgCo compound is detected. This result indicates that the reactivity of the Mg–Co system with 1:1 composition after cycling under 2 MPa of hydrogen tends to formation of Mg_2CoH_5 over other hydride phases, i.e. MgH_2 and $Mg_6Co_2H_{11}$.

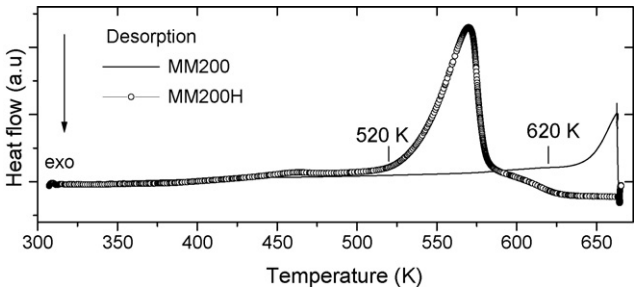

Fig. 5. HP-DSC curves during desorption reaction of MM200 (—) and MM200H (–o–). Heating rate 5 K min^{-1}; under vacuum.

To further clarify the absorption/desorption paths, XRD analyses were performed after each cycle. In the activation cycle of the MM200, minor amount of $Mg_6Co_2H_{11}$ was detected simultaneously with Mg_2CoH_5 as major phase (not shown). After a desorption step under vacuum up to 673 K leads to the formation of MgCo compound, with Mg and Co as residual phases (not shown) its formation can be associated with the Mg–Co solid-state reaction at 673 K and/or the decomposition of $Mg_6Co_2H_{11}$/Mg_2CoH_5 [4–6,9–12]. On the other hand, first cycle of MMH200 is similar to the second cycle of MM200, in relation with both hydrogen absorption behavior (exothermic peak at about 420 K) and the phases formed due to Mg–Co–H reaction. Clearly, the presence of MgCo compound in the starting MM200H sample is equivalent with the first absorption/desorption cycle of MM200.

Two relevant aspects need additional analysis. One of them is the reduction of 100 K in the hydrogen desorption temperature in MM200H respect to MM200. The main difference between these samples is the presence of MgCo in the MM200H starting mixture that improves the kinetics and the amount of Mg_2CoH_5 formation *via* MgCo compound. We believe that MgCo formation is an evidence of good Mg–Co homogenization during thermal treatment. Thus, the desorption peak observed in Fig. 5 for MM200H is due to the decomposition of Mg_2CoH_5 (the only hydride phase) in the presence of free Co, which could act as catalyst for the hydrogen recombination during desorption [9–11,14].

The second interesting result is the increment (reduction) of the heat flow associated with the first peak after cycling for MM200 (MM200H). A possible explanation of this behavior is in connection with the amount of MgCo in the sample. For the starting MM200H sample, the MgCo amount obtained after solid-state reaction is practically the maximum for 1:1 Mg–Co composition (residual Mg/Co phases are undetectable, see Fig. 2b). However, MgCo amount after desorption up to 673 K is lower, whereas the most intense Mg and Co diffractions are clearly identified (not shown). Then, the absorption peak area decreases for the sample MM200H after cycling. In opposition, in the MM200 sample the amount of MgCo increases due to activation on cycling of Mg–Co mixture. Therefore, the amount of MgCo obtained after desorption from hydride decomposition is relevant to the further reactivity with hydrogen and is dependent of the thermal history of the sample. Additional measurements will be performed to clarify this behavior in relation with the reversibility of MgCo to Mg_2CoH_5 reaction.

4. Conclusions

Mechanical milling of Mg–Co mixture improves the refinement of the microstructure and Mg–Co intermixing. These microstructural characteristics allow the formation of MgCo at 573 K, the lowest temperature reported for this intermetallic.

The presence of MgCo in the starting sample (MM200H) has a great influence on the reactivity with hydrogen. Hydrogen absorption in the first cycle is higher than the corresponding to the Mg–Co mixture with Mg and Co phases (MM200). In addition, temperature desorption is decreased in 100 K, in connection with the hydriding/dehydriding of MgCo/Mg_2CoH_5. Moreover, cycling under hydrogen of the Mg–Co as-milled and as-heated samples leads to the formation of Mg_2CoH_5 *via* MgCo, despite thermodynamic data allow the existence of different hydride phases: MgH_2, Mg_2CoH_5 and $Mg_6Co_2H_{11}$. Thus, local compositional homogenization reached under hydrogen cycling/thermal treatment determines the amount of MgCo formed and the further hydriding/dehydriding characteristics. Understanding the MgCo role on the hydride formation will be useful to establish experimental conditions that maximize technological properties for hydrogen storage applications.

Acknowledgments

The authors thank CONICET and ANPCyT for partial financial support to carry out this work.

References

[1] T. Massalski, H. Okamoto, P. Subramanian, L. Kacprzak (Eds.), Binary Alloy Phase Diagrams, 2nd ed., American Society for Metals, Metals Park, OH, 1990.
[2] A.A. Nayeb-Hashemi, J.B. Clark, Bull. Alloy Phase Diagrams 8 (1987) 352–355.
[3] P. Zolliker, K. Yvon, P. Fisher, J. Schefer, Inorg. Chem. 24 (1985) 4177–4180.
[4] E.J. Ivanov, I.G. Konstanchuk, A. Stepanov, M. Yan Jie, B. Pezat, Darriet, Inorg. Chem. 28 (1989) 613–615.
[5] M. Yoshida, F. Bonhomme, K. Yvon, P. Fischer, J. Alloys Compd. 190 (1993) L45–L46.
[6] F.C. Gennari, F. Castro, J. Alloys Compd. 396 (2005) 182–192.
[7] R. Černý, F. Bonhomme, K. Yvon, P. Fisher, P. Zolliker, D.E. Cox, A. Hewat, J. Alloys Compd. 187 (1992) 233–241.
[8] G. Meyer, D.S. Rodríguez, F. Castro, G. Fernández, Proceedings of the 11th World Energy Conference, Stuttgart, vol. 2, 1996, pp. 1293–1297.
[9] I. González Fernández, G.O. Meyer, F.C. Gennari, J. Alloys Compd. 446–447 (2007) 106–109.
[10] I. González Fernández, F.C. Gennari, G.O. Meyer, J. Alloys Compd. 462 (2008) 119–124.
[11] I. González Fernández, G.O. Meyer, F.C. Gennari, J. Alloys Compd. 464 (2008) 111–117.
[12] H. Shao, H. Xu, Y. Wang, X. Li, J. Solid State Chem. 177 (2004) 3626–3632.
[13] C. Rongeat, I. Llamas, S. -Jansa, S. Doppiu, A. Deledda, L. Borgschulte, O. Schultz, Gutfleisch, J. Phys. Chem. B 111 (2007) 13301–13306.
[14] N. Hanada, T. Ichikawa, H. Fujii, J. Phys. Chem. B 109 (2005) 7188–7194.